

Dynamical decoupling and dynamical isolation in temporally modulated coupled pendulums

GRAZIA SALERNO and IACOPO CARUSOTTO

INO-CNR BEC Center and Dipartimento di Fisica, Università di Trento, via Sommarive 14, 38123 Povo, Italy

PACS 45.20.D--Newtonian mechanics
 PACS 46.40.Ff--Resonance, damping, and dynamic stability
 PACS 03.65.Vf--Phases: geometric; dynamic or topological

Abstract –We theoretically study the dynamics of a pair of coupled pendulums subject to a periodic temporal modulation of their oscillation frequency. Inspired from analogous developments in quantum mechanics, we anticipate dynamical localization and dynamical isolation effects, as well as the occurrence of non-trivial coupling phases. Perspectives in the direction of studying synthetic gauge fields in a classical mechanics context are outlined.

Introduction. – Dynamical localization is a surprising consequence of quantum mechanics applied to particles moving in periodic potentials and subject to a strong time-dependent external force. This effect was first predicted in a solid state context [1–3]: when a strong a.c. field is applied to a metal, its conductivity in response to a weak d.c. field is anticipated to be dramatically suppressed for certain values of the a.c. field amplitude. A closely related effect is the coherent destruction of tunneling in a double-well geometry, first predicted in [4, 5].

While the experimental study of these effects in solids is made difficult by the unavoidable material imperfections and electronic decoherence, the robust coherence and the clean periodic potential experienced by atomic matter waves in temporally modulated optical lattices has allowed for a clear observation of Bloch band suppression in a new atomic physics context [6]. Further studies of dynamical matter wave localization effects were reported in [7, 8] using Bose-condensed atomic samples. Following the proposal [9, 10], this research line culminated in the observation of a dynamically-induced superfluid to Mott-insulator transition [11].

Very exciting further developments of these ideas aim at using more complex modulation schemes to generate non-trivial hopping phases between the lattice sites [12, 13] and then synthetic gauge fields for neutral atoms [14–17]. Correspondingly to these advances in atomic physics, the same ideas are being explored in photonics to observe dynamical localization of light in coupled optical waveguides [18] and, very recently, to generate synthetic gauge field for photons [19].

In this Letter, we report a theoretical study of dynamical localization phenomena in a classical mechanics context. The dynamic stabilization of the inverted pendulum when its pivot point is made to oscillate in space is a well celebrated example of non-trivial mechanical effect stemming from a temporal modulation of the system parameters [20]. Here we consider a system of two coupled pendulums, whose oscillation frequencies are independently and periodically varied in time. In analogy to the coherently suppressed tunneling of a quantum particle in a double-well potential, we predict a *dynamical decoupling* effect, where exchange of energy between the two pendulums is suppressed. When the pendulums are driven by an external force, a novel *dynamic isolation* effect is anticipated, where the temporal modulation effectively decouples the system from the external driving.

The system and the theoretical model. – The system of two identical coupled pendulums is modelled as a pair of coupled harmonic oscillators of equal masses m following the motion equations:

$$m \dot{x}_1 = p_1 \quad (1)$$

$$\dot{p}_1 = -m\omega_0^2 [1 + \nu_1(t)] x_1 + k(x_2 - x_1) - \xi_1 \dot{x}_1 \quad (2)$$

$$m \dot{x}_2 = p_2 \quad (3)$$

$$\dot{p}_2 = -m\omega_0^2 [1 + \nu_2(t)] x_2 + k(x_1 - x_2) - \xi_2 \dot{x}_2. \quad (4)$$

The $x_{1,2}$ variables indicate the spatial displacement of the pendulums from the equilibrium position. The linearized form of the motion equations is legitimate in the small oscillation regime where the displacements are much

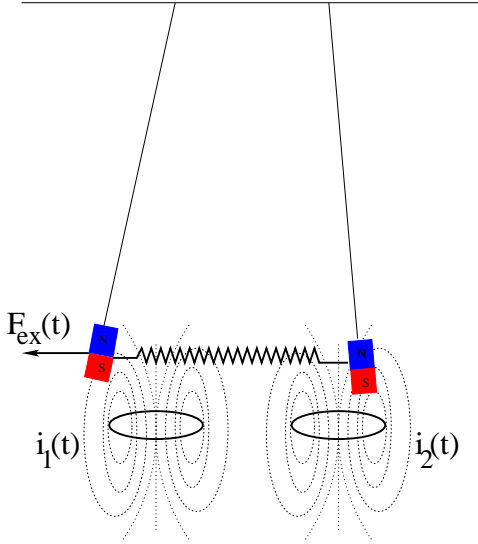


Figure 1: Sketch of the physical system under consideration. Each pendulum contains a magnetized element and the modulation of the oscillation frequency of each pendulum is controlled by the time-dependent current $i_{1,2}(t)$ flowing in the coil located under the pendulum. The first pendulum may be externally driven by a time-dependent force $F_{\text{ex}}(t)$.

smaller than the length L of the pendulums, $|x_{1,2}| \ll L$: in this regime, the natural oscillation frequency of each isolated pendulum is the usual $\omega_0 = \sqrt{g/L}$. The friction constants of the two pendulums have the same value $\xi_1 = \xi_2$. The coupling between the pendulums occurs via a spring of constant k .

The key element to achieve the dynamical localization and dynamical isolation effects is the temporal modulation of the system, which is included in Eq. (2) and Eq. (4) as a temporal modulation of the restoring force strengths of relative amplitude $\nu_{1,2}(t)$. One of the possible concrete realizations of this model is sketched in Fig. 1: each pendulum contains a magnet which feels the magnetic field generated by a coil located below its axis. In this way, the gravitational restoring force felt by each pendulum is supplemented by a contribution of magnetic origin, which can be controlled via the (time-dependent) current $i_{1,2}(t)$ flowing in the corresponding coil. The effective modulation of the natural oscillator frequencies is then described by the following:

$$\omega_{1,2}^2(t) = \omega_0^2 [1 + \nu_{1,2}(t)], \quad (5)$$

with the parameters $\nu_{1,2}(t)$ proportional to the currents $i_{1,2}(t)$.

The four equations of motion Eqs. (1)-(4) can be summarized in a pair of complex equations:

$$\begin{aligned} \dot{\alpha}_i = & -i\omega_0 \alpha_i - i\nu_i(t)(\alpha_i + \alpha_i^*) - \gamma_i(\alpha_i - \alpha_i^*) \\ & + i\frac{\Omega}{2}(\alpha_{3-i} + \alpha_{3-i}^* - \alpha_i - \alpha_i^*). \end{aligned} \quad (6)$$

for the $\alpha_{i=1,2}$ complex variables defined as:

$$\alpha_i = \sqrt{\frac{m\omega_0}{2}} x_i + i\sqrt{\frac{1}{2m\omega_0}} p_i. \quad (7)$$

Complex conjugate equations hold for the $\alpha_{1,2}^*$. For notational simplicity, we have also introduced the rescaled quantities:

$$v_{1,2}(t) = \frac{\nu_{1,2}(t)\omega_0}{2}, \quad \Omega = \frac{k}{m\omega_0}, \quad \gamma_{1,2} = \frac{\xi_{1,2}}{2m}.$$

In order for the coupling between the oscillators to be effective, the strong coupling $\Omega \gg \gamma_i$ condition will be assumed. In the following we shall concentrate our attention on sinusoidal modulations of the form:

$$v_i(t) = (-1)^i I_0 \sin(\omega t) \quad (8)$$

where the modulations for the two pendulums have the same frequency ω but opposite phases. As we shall see better in the following of this Letter, a most convenient regime where to obtain and observe the dynamical localization physics is characterized by the inequality chain:

$$\omega_0 \gg \omega \gg \Omega. \quad (9)$$

The latter inequality is essential to describe the system in terms of an effective, time-averaged coupling. The former inequality helps to reduce those parametric instabilities that might otherwise occur for large values of the modulation amplitude I_0 [21, 22].

Dynamical decoupling of the oscillators. – As a preliminary step, we have numerically integrated Eq. (6) in the vanishing friction case, $\gamma_{1,2} = 0$. The integration method is a standard fourth order Runge-Kutta. In Fig. 2 we have plotted the evolution of the $|\alpha_{1,2}|$ sampled at periodically spaced times $T_j = 2\pi j/\omega$ with the frequency ω of the modulation. When only these stroboscopic times are considered, the system is described by a time-independent discrete evolution law. The different panels of Fig. 2 correspond to the same modulation frequency ω but different values of the amplitude I_0 .

In panel (a), there is no modulation, $I_0 = 0$: the amplitudes of the two oscillators exhibit the usual beating phenomena, *i.e.* a periodic exchange of energy between the oscillators at the coupling frequency Ω . For increasing values of the modulation amplitude I_0 , the frequency of the beating is modified as a result of the modulation $\nu_i(t)$: in particular, for the parameters of panels (b) and (c), the beating frequency is more and more reduced. For even larger amplitudes I_0 , a non-monotonic behaviour of the effective beating frequency is observed (not shown).

Experimental proposal and dynamical isolation. –

In order to perform a quantitative study of the effect of the modulation and, at the same time, to propose a viable procedure to experimentally observe these phenomena, it is useful to consider the realistic case of dissipative pendulums driven by an external force. While the

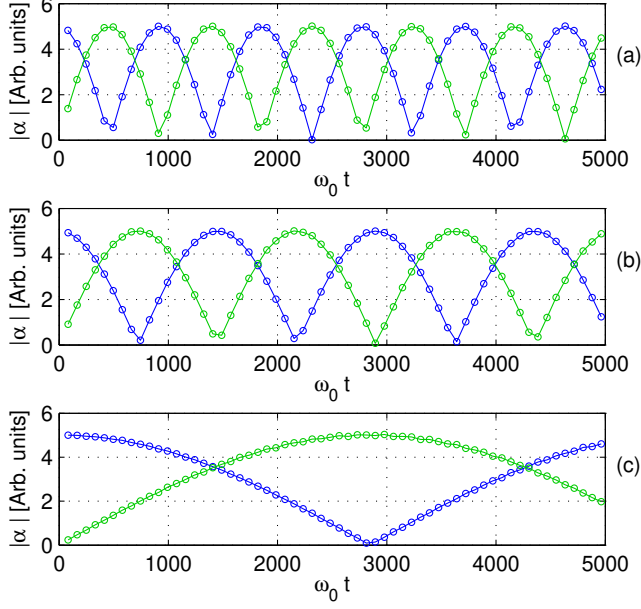


Figure 2: Result of the numerical integration of the equations of motion Eq. (6). The blue (green) dots indicate the modulus $|\alpha_1|$ ($|\alpha_2|$) of the oscillation amplitude of the first (second) pendulum in arbitrary units. At the initial time, the excitation is located on the first oscillator, $\alpha_1(t=0) = 5$ arb. u. and $\alpha_2(t=0) = 0$ arb. u.. The evolution of the two pendulums is stroboscopically followed at the modulation frequency w , while the lines are guides to the eyes. The three panels are for different values of the modulation amplitude, $I_0/w = 0$ (a), $I_0/w = 0.632$ (b), and $I_0/w = 1.053$ (c). System parameters are $w/\omega_0 = 7.6 \times 10^{-2}$, $\Omega/\omega_0 = 0.68 \times 10^{-2}$, $\gamma_{1,2}/\omega_0 = f_{\text{ex}}/\omega_0 = 0$.

(weak) dissipation affects both pendulums with the same rate $\gamma_1 = \gamma_2 \ll \Omega$, the external force is assumed to be monochromatic, $F_{\text{ex}}(t) = 2f_{\text{ex}} \cos \omega_{\text{ex}} t$ and to act on the first pendulum only. Energy transfer to the second pendulum is made possible by the spring that couples the two pendulums. The driven-dissipative motion equations then take the form:

$$\begin{aligned} \dot{\alpha}_1 = & -i(\bar{\omega}_0 - i\gamma_1)\alpha_1 - i v_1(t)(\alpha_1 + \alpha_1^*) \\ & - i\left(\frac{\Omega}{2} + i\gamma_1\right)\alpha_1^* + i\frac{\Omega}{2}(\alpha_2 + \alpha_2^*) + iF_{\text{ex}}(t) \end{aligned} \quad (10)$$

and

$$\begin{aligned} \dot{\alpha}_2 = & -i(\bar{\omega}_0 - i\gamma_2)\alpha_2 - i v_2(t)(\alpha_2 + \alpha_2^*) \\ & - i\left(\frac{\Omega}{2} + i\gamma_2\right)\alpha_2^* + i\frac{\Omega}{2}(\alpha_1 + \alpha_1^*) \end{aligned} \quad (11)$$

where we have defined the short-hand $\bar{\omega}_0 = \omega_0 + \Omega/2$.

The response spectra of each pendulum as a function of the frequency of the external force ω_{ex} are shown in Fig. 3 for a fixed amplitude of the driving force: for each ω_{ex} , the equations of motion Eqs. (10)-(11) have been integrated until a steady-state regime, showing regular periodic oscillations, is achieved at long times $t \gg 1/\gamma_i$. For

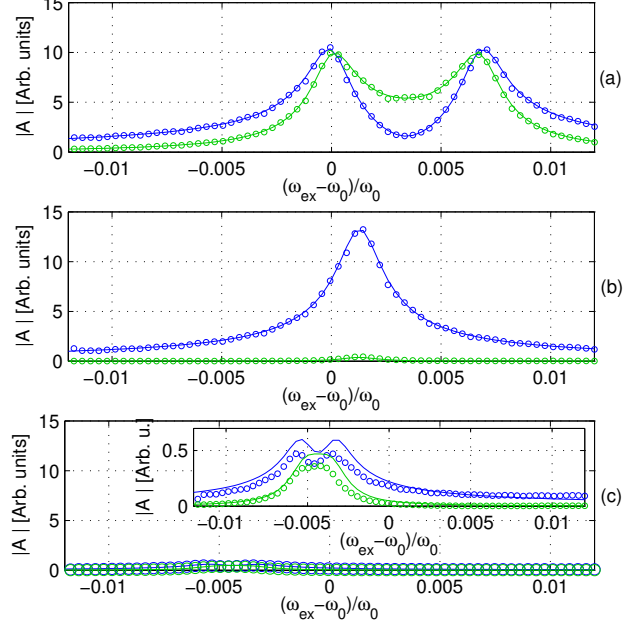


Figure 3: Numerical response spectra as a function of the frequency ω_{ex} of the external force. The modulus $|A(\omega_{\text{ex}})|$ of the oscillation amplitude of the stroboscopically sampled solution is shown for the first (second) pendulum as blue (green) dots, in arbitrary units. The different panels corresponds to different values of the modulation amplitude, $I_0/w = 0$ (a), $I_0/w = 1.21$ (b), $I_0/w = 2.31$ (c). The inset in (c) shows an enlargement of the main plot. The solid lines show the result of an analytical calculation based on the rotating-wave approximation (see text). System parameters: $w/\omega_0 = 7.6 \times 10^{-2}$, $\Omega/\omega_0 = 0.68 \times 10^{-2}$, $\gamma_{1,2}/\omega_0 = 0.1 \times 10^{-2}$, $f_{\text{ex}}/\omega_0 = 4 \times 10^{-2}$.

the stroboscopic sampling at times $t = T_j = 2\pi j/w$, the steady oscillation has the form:

$$\alpha_i(t) \approx A_i(\omega_{\text{ex}}) e^{-i\omega_{\text{ex}} t}. \quad (12)$$

The (complex) amplitudes A_i , whose moduli are plotted in Fig. 3, are obtained via a Fourier transformation of the stroboscopically sampled numerical solutions. Each panel of the figure corresponds to a different value of the modulation amplitude I_0 and illustrates a different regime.

The standard behaviour is shown in panel (a) for the $I_0 = 0$ case of no modulation: as expected, the spectra are characterized by a pair of peaks split by Ω and of equal widths $\gamma_{1,2}$. The lower- (upper-) frequency peak corresponds to the eigenmode of the system where the two pendulums oscillate with the same (opposite) phase. At all frequencies, the oscillation amplitudes of the two pendulums remain comparable.

Panel (b) shows the case where the coupling of the two pendulums is dramatically suppressed: this effect is apparent in the figure as the two peaks merge into a single peak and no significant excitation is transferred to the second pendulum, which remains basically at rest with a negligible oscillation amplitude. This behaviour is the

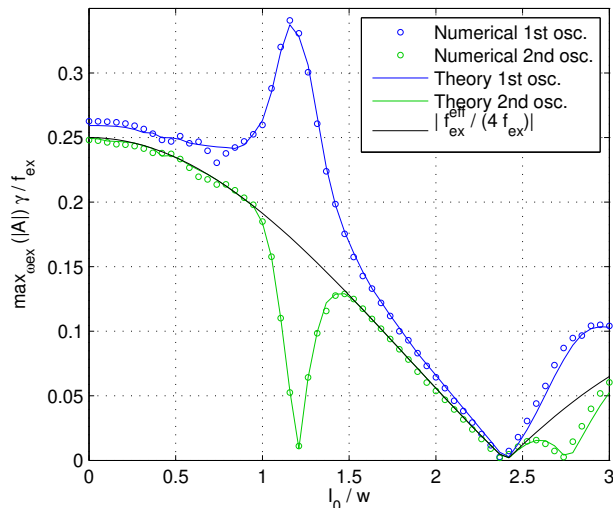


Figure 4: Blue (green) dots show the normalized maximum of the oscillation amplitude for the first (second) oscillator as a function of the normalized modulation amplitude I_0 . The solid lines show the result of an analytical calculation based on the rotating-wave approximation (see text). System parameters as in Fig. 3.

driven-dissipative manifestation of the *dynamical decoupling* effect, already seen in the lowest panel of Fig. 2.

Panel (c) shows a novel regime: while some (reduced) effective coupling of the two pendulums is still present, their global excitation by the external force is suppressed. The suppressed excitation is visible as a very small oscillation amplitude of both pendulums. The presence of a significant coupling is apparent in the inset where the response of the first pendulum is still showing a clear doublet.

These different regimes are illustrated in more detail in Fig. 4. Response spectra like the ones in Fig. 3 have been numerically calculated for a number of different values of the modulation amplitude I_0 . For each of these values, in panel (a) of Fig. 4, we plot the maximum of the amplitude $|A_i(\omega_{ex})|$ over the drive frequency ω_{ex} , that is the resonant response at the peaks. The dynamical decoupling seen in Fig. 3(b) corresponds here to the minimum of $\max(|A_2|)$ that is visible around $I_0/w \simeq 1.2$. The dynamical isolation seen in Fig. 3(c) lies in the vicinity of the simultaneous minima of both $\max(|A_{1,2}|)$ that are visible around $I_0/w \simeq 2.4$. In the figure, note the further dynamical decoupling point around $I_0/w \simeq 2.7$. The solid lines are the analytical predictions of the rotating wave approximation that will be presented in the next section.

Further insight on the effective coupling of the two pendulums, resulting from the temporal modulation, is given in Fig. 5. In the upper panel (a) we present the numerically estimated magnitude of the effective coupling between the pendulums: this quantity is observable as the exchange rate of energy between the two pendulums,

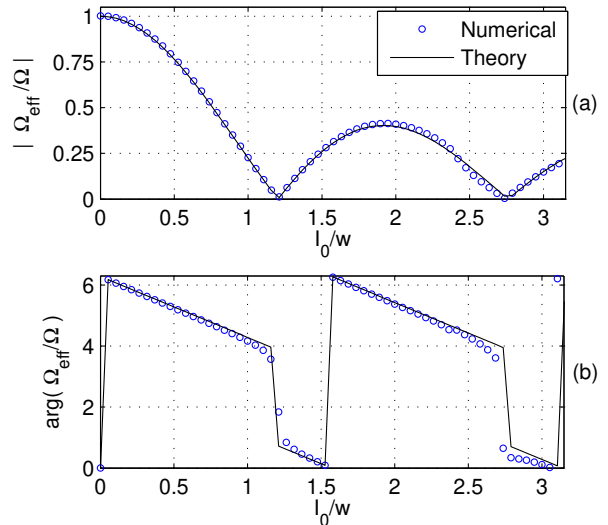


Figure 5: Plot of the modulus of the effective coupling frequency $|\Omega_{\text{eff}}|/\Omega$ [upper (a) panel] and of its phase $\arg(\Omega_{\text{eff}})$ (modulo 2π) [lower (b) panel]. Dots are the result of the numerical calculations as discussed in the text while the solid line is the analytical prediction of the rotating wave approximation. System parameters as in Fig. 3.

studied in Fig. 2, or as the separation between peaks in the response spectra of Fig. 3. Most remarkable features of Fig. 5(a) are the vanishing effective coupling at $I_0/w \simeq 1.2$ and $I_0/w \simeq 2.7$, corresponding to the zeros of only $|A_2|$ in Fig. 4(a).

Another crucial consequence of the temporal modulation is shown in the lower panel Fig. 5(b). While the eigenmodes of the bare system correspond to in- and opposite-phase oscillations, the modulation allows to tune the relative phase of the oscillation of the two pendulums to any value from 0 to 2π . In mathematical terms, the effective coupling develops a non-trivial phase, as shown in the figure. Note in particular how this phase displays π jumps whenever the effective coupling goes through zero. Before proceeding, it is worth noting in Fig. 3 a sizeable global shift of the resonance curves towards lower frequencies for growing I_0 . An explanation of this effect will be given in the next section.

Analytical expressions within the rotating wave approximation. – Analytical insight in the physics of the modulated system can be obtained within the so-called rotating wave (RW) approximation, well-known from quantum optics. This approximation relies on assuming that the natural oscillation frequency ω_0 is much larger than all other internal frequencies in the problem, that is $\omega_0 \gg \max(\Omega, \gamma_i, w, |\omega_{ex} - \omega_0|)$. Since the α variables rotate at $\approx \omega_0$ and their conjugate variables α^* rotate at $\approx -\omega_0$, the RW approximation is straightforwardly implemented by neglecting the α^* terms in the motion Equations (10)-(11) for the α variables.

To obtain an effective, temporally averaged form of the stroboscopic dynamics of the system, it is convenient to introduce the following new variables:

$$\beta_i(t) = \alpha_i(t) e^{i \int_0^t v_i(t') dt'} e^{i\omega_{\text{ex}} t}. \quad (13)$$

For the chosen sinusoidal form of the modulation, the phase factor involving the modulation is exactly equal to 1 at the stroboscopic times $t = T_j = 2\pi j/w$ that are considered in the figures. Assuming that the modulation frequency w is much faster than the coupling one Ω , effective equations, which no longer depend on the time t , can be obtained [23] by averaging the RW form of the equations (10)-(11) over a modulation period $T = 2\pi/w$:

$$\dot{\beta}_1 = -i(\bar{\omega}_0 - \omega_{\text{ex}}) \beta_1 - \gamma_1 \beta_1 + i \frac{\Omega_{12}^{\text{eff}}}{2} \beta_2 + i f_{\text{ex}}^{\text{eff}} \quad (14)$$

$$\dot{\beta}_2 = -i(\bar{\omega}_0 - \omega_{\text{ex}}) \beta_2 - \gamma_2 \beta_2 + i \frac{\Omega_{21}^{\text{eff}}}{2} \beta_1. \quad (15)$$

The effective averaged couplings that appear in Eqs. (14)-(15) are defined by:

$$\Omega_{ij}^{\text{eff}} = \frac{\Omega}{T} \int_0^T dt e^{i \int_0^t [v_i(t') - v_j(t')] dt'}.$$

and they are complex conjugate to each other, $\Omega_{12}^{\text{eff}} = \Omega_{21}^{\text{eff}*}$, therefore we can introduce the quantity $\Omega_{\text{eff}} = \Omega_{12}^{\text{eff}}$. For the specific modulation considered here, the effective coupling has the simple expression:

$$\Omega_{\text{eff}} = \Omega e^{-2iI_0/w} \mathcal{J}_0(2I_0/w) \quad (16)$$

in terms of the \mathcal{J}_0 zero-order Bessel function. The modulus and the phase of this quantity are plotted as a solid line in Fig. 5. In particular, the modulus $|\Omega_{\text{eff}}|$ shows a series of zeros, which are indicative of a complete *dynamical decoupling* between the two pendulums.

The same procedure must be applied to the amplitude of the external driving force in Eq. (14), which gives the effective averaged driving force:

$$f_{\text{ex}}^{\text{eff}} = \frac{f_{\text{ex}}}{T} \int_0^T dt e^{i \int_0^t v_i(t') dt'}$$

that, for the specific modulation in Eq. (8), has the explicit form:

$$f_{\text{ex}}^{\text{eff}} = f_{\text{ex}} e^{-iI_0/w} \mathcal{J}_0(I_0/w) \quad (17)$$

The zeros of this quantity determine the parameter values at which complete *dynamical isolation* from the external driving force is found.

Explicit forms for the steady oscillation regime can be derived by setting the time derivatives in Eqs. (14)-(15) to zero. In this way, one obtains the following analytical

form of the resonance curves as function of ω_{ex} :

$$\beta_1(\omega_{\text{ex}}) = \frac{f_{\text{ex}}^{\text{eff}} (\bar{\omega}_0 - i\gamma_2 - \omega_{\text{ex}})}{2(\bar{\omega}_0 - i\gamma_1 - \omega_{\text{ex}})(\bar{\omega}_0 - i\gamma_2 - \omega_{\text{ex}}) - \frac{|\Omega_{\text{eff}}^{\text{eff}}|^2}{2}} \quad (18)$$

$$\beta_2(\omega_{\text{ex}}) = \frac{f_{\text{ex}}^{\text{eff}} \Omega_{\text{eff}}^*}{4(\bar{\omega}_0 - i\gamma_1 - \omega_{\text{ex}})(\bar{\omega}_0 - i\gamma_2 - \omega_{\text{ex}}) - |\Omega_{\text{eff}}^{\text{eff}}|^2}. \quad (19)$$

While a qualitative agreement with the numerical predictions shown in Fig. 3 is already present at this level, there is still an overall global shift of the resonances. This shift is easily explained by including the leading order correction to the RW approximation. We allow for the α_i to also have a small counter-rotating part evolving at frequency $-\omega_{\text{ex}}$ by writing $\alpha_i(t) = \alpha_i^{\text{rw}} e^{-i\omega_{\text{ex}} t} + \delta\alpha_i^{\text{nrw}} e^{i\omega_{\text{ex}} t}$. Since the α and the α^* are coupled by the non-RW terms in Eqs. (10)-(11) and their complex conjugate equations, counter-rotating contributions appear in the equation for α from the counter-rotating terms of α^* . The magnitude of these correction is largest for the term proportional to v_i , to which we will restrict for simplicity. A straightforward calculation gives $\delta\alpha_i^{\text{nrw}} \simeq -(\alpha_i^{\text{rw}})^* v_i(t)/(2\omega_0)$. After substituting this expression into Eq. (10) and isolating the non-rotating terms, we are left with the (time-dependent) frequency shift: $\Delta\omega_0 = -v_i^2(t)/(2\omega_0)$. By averaging over the modulation period of the considered modulation, the effective averaged frequency shift:

$$\Delta\omega_0 = -\langle v_i(t)^2 \rangle_T / (2\omega_0) = -I_0^2 / (4\omega_0) \quad (20)$$

is obtained. This is the principal effect of the counter-rotating terms beyond the RW, and it is more and more important for growing I_0 . All other non-RW contributions involving Ω and γ_i are instead negligible for the chosen parameters. The shift $\Delta\omega_0$ can be taken into account in Eqs. (18)-(19) by replacing $\bar{\omega}_0$ with $\tilde{\omega}_0 = \bar{\omega}_0 + \Delta\omega_0$. In this way, an excellent agreement for the analytical spectra (solid lines) with the result of the numerical simulations (dots) is found in Fig. 3.

This suggests a way to extract an estimate of the effective coupling Ω_{eff} from the numerical results. An explicit expression of it in terms of the oscillation amplitudes is obtained by taking the ratio of Eq. (18) and Eq. (19):

$$\Omega_{\text{eff}} = 2(\tilde{\omega}_0 + i\gamma - \omega_{\text{ex}}) \left(\frac{\beta_2}{\beta_1} \right)^*. \quad (21)$$

The result of replacing in this equation the β_i with the numerically calculated A_i is shown by the dots in Fig. 5 and is compared with the analytical RW prediction of Eq. (16). The agreement appears to be very good for both the magnitude and the phase of the coupling, in particular the position of the dynamical decoupling points at which $\Omega_{\text{eff}} = 0$. The small discrepancies occur when both numerator and denominator of Eq. (21) go to zero and the procedure is more sensitive to numerical errors.

A similar comparison for the effective driving force is performed in Fig.4, where the numerical results are compared to RW prediction of Eq. (17) renormalized to the peak amplitude of Eqs. (18)-(19) in the small $\gamma_1 = \gamma_2$ limit. The agreement is again very good, in particular for what concerns the position of the dynamical isolation points for which $f_{\text{ex}}^{\text{eff}} = 0$ and both $\max(|A_{1,2}|) = 0$. Of course, the agreement gets worse when the pendulum frequency approaches the other frequency scales and the inequality chain of Eq. (9) is only marginally satisfied.

Connection to the Bose-Hubbard model. – Before concluding, it is worth to highlight the direct connection of the RW description of the system of coupled pendulums to a driven-dissipative version of the Bose-Hubbard (BH) model of quantum condensed-matter. In the presence of an external gauge field [24], the BH model is described by the Hamiltonian:

$$\hat{\mathcal{H}} = - \sum_{\langle ij \rangle} \left[J e^{i\phi_{ij}} \hat{a}_i^\dagger \hat{a}_j + \text{h.c.} \right] + \sum_i \frac{U}{2} \hat{a}_i^\dagger \hat{a}_i^\dagger \hat{a}_i \hat{a}_i \quad (22)$$

where \hat{a}_i and \hat{a}_i^\dagger are bosonic on-site operators. The first term describes hopping of the bosonic particles: the hopping amplitude is J and the phase ϕ_{ij} describes a non-trivial tunneling phase. Of course, non-rotating wave terms do not appear in the standard condensed-matter BH model Hamiltonian in Eq. (22) as they would correspond to processes where the total numbers of particles is not conserved. If particles are instead injected from a coherent source and lost from the system, the theoretical description requires adding a driving term of the form $\hat{\mathcal{H}}_F = \sum_i [f_{\text{ex},i}(t) \hat{a}_i^\dagger + \text{h.c.}]$ as well as damping terms, to be typically included at the level of the master equation [25].

Under the classical approximation where operators are replaced by \mathbb{C} numbers, equations of motion analogous to Eqs. (18)-(19) are found. In particular, the complex hopping amplitude of the BH model corresponds to the complex coupling between the pendulums, $J e^{i\phi_{ij}} \longleftrightarrow \Omega_{ij}^{\text{eff}}$: the non-trivial Peierls phase $\phi_{ij} = \int_{r_j}^{r_i} \text{dr} \cdot \mathbf{A} / \hbar$ describing the effect of an external vector potential acting on the quantum particles [24] corresponds to a non-trivial phase of the Ω_{ij}^{eff} coupling. An on-site interaction term analogous to the U term in Eq. (22) directly appears when the anharmonicity of the pendulums is taken into account beyond the linearized motion Equations (1)-(4).

The modulation scheme that has been envisaged in the present Letter for coupled pendulums corresponds to a temporal modulation of the on-site energies of the BH lattice. There is however one crucial difference worth noting: while the global shaking of the optical lattice potential that is typically used for this purpose in ultracold atom experiments [6, 7, 11, 13] can only provide modulation amplitudes that are linearly dependent on the site position [23], systems of pendulums allow for an individual addressing of each single pendulum. This freedom will be very useful in view of generating synthetic gauge

field configurations in our mechanical system [15].

Final remarks and conclusions. – Inspired by analogous quantum effects, in this Letter we have theoretically studied dynamical localization and dynamical isolation effects in a classical system of two coupled pendulums when a temporally periodic modulation of the oscillation frequencies is applied to the pendulums. The dynamical decoupling effect can be used in mechanical engineering to suppress the coupling between the two pendulums, while the dynamical isolation allows to isolate the system from external forces. Of course, our results are valid for coupled oscillators of any physical nature with a time dependent frequency, for instance temporally modulated RLC electric circuits.

From the point of view of fundamental physics, the non-trivial coupling phase between the pendulums is analogous to the Peierls phase of bosonic Hubbard models of quantum condensed-matter physics. In analogy to orbital magnetism and topological insulation, new intriguing phenomena are expected to appear in multi-dimensional lattices of many temporally modulated pendulums. Further exciting developments in nonlinear physics are expected to arise as a result of the intrinsic anharmonicity of pendulums.

* * *

We are grateful to Nicola Pugno, André Eckardt and Jean Dalibard for stimulating discussions. We acknowledge partial financial support from ERC via the QGBE grant and from Provincia Autonoma di Trento.

References

- [1] DUNLAP D. H. and KENKRE V. M., *Phys. Rev. B*, **34** (1986) 3625.
- [2] ZHAO X.-G., *J. Phys.*, **6** (1994) 2751.
- [3] HOLTHAUS M., *Phys. Rev. Lett.*, **69** (1992) 351.
- [4] GROSSMANN F., DITTRICH T., P. JUNG and HÄNGGI, *Phys. Rev. Lett.*, **67** (1991) 516.
- [5] GRIFONI M. and HÄNGGI P., *Phys. Rep.*, **304** (1998) 229.
- [6] MADISON K. W., FISCHER M. C., DIENER R. B., NIU Q. and RAIZEN M. G., *Phys. Rev. Lett.*, **81** (1998) 5093.
- [7] LIGNIER H., SIAS C., CIAMPINI D., SINGH Y., ZENESINI A., MORSCH O. and ARIMONDO E., *Phys. Rev. Lett.*, **99** (2007) 220403.
- [8] ECKARDT A., HOLTHAUS M., LIGNIER H., ZENESINI A., CIAMPINI D., MORSCH O. and ARIMONDO E., *Phys. Rev. A*, **79** (2009) 013611.
- [9] ECKARDT A., WEISS C. and HOLTHAUS M., *Phys. Rev. Lett.*, **95** (2005) 260404.
- [10] ECKARDT A. and HOLTHAUS M., *Europhys. Lett.*, **80** (2007) 50004.
- [11] ZENESINI A., LIGNIER H., CIAMPINI D., MORSCH O. and ARIMONDO E., *Phys. Rev. Lett.*, **102** (2009) 100403.
- [12] CREFFIELD C. E. and SOLS F., *Phys. Rev. Lett.*, **100** (2008) 250402.

- [13] STRUCK J., ÖLSCHLÄGER C., WEINBERG M., HAUKE P., SIMONET J., ECKARDT A., LEWENSTEIN M., SENGSTOCK K. and WINDPASSINGER P., *Phys. Rev. Lett.*, **108** (2012) 225304.
- [14] KOLOVSKY A. R., *Europhys. Lett.*, **93** (2011) 20003.
- [15] CREFFIELD C. E. and SOLS F., *Europhys. Lett.*, **101** (2013) 40001.
- [16] HAUKE P., TIELEMAN O., CELI A., ÖLSCHLÄGER C., SIMONET J., STRUCK J., WEINBERG M., WINDPASSINGER P., SENGSTOCK K., LEWENSTEIN M. and ECKARDT A., *Phys. Rev. Lett.*, **109** (2012) 145301.
- [17] STRUCK J., WEINBERG M., ÖLSCHLÄGER C., WINDPASSINGER P., SIMONET J., SENGSTOCK K., HÖPPNER R., HAUKE P., ECKARDT A., LEWENSTEIN M. and MATHEY L., *Nat. Phys.*, **9** (2013) 738.
- [18] LONGHI S., MARANGONI M., LOBINO M., RAMPONI R., LAPORTA P., CIANCI E. and FOGLIETTI V., *Phys. Rev. Lett.*, **96** (2006) 243901.
- [19] RECHTSMAN M. C., ZEUNER J. M., PLOTNIK Y., LUMER Y., PODOLSKY D., DREISOW F., NOLTE S., SEGEV M. and SZAMEIT A., *Nat.*, **496** (2013) 196.
- [20] BUTIKOV E. I., *Am. J. Phys.*, **69** (2001) 755.
- [21] ARNOLD V.I., *Mathematical Methods of Classical Mechanics* (Springer-Verlag, New York) 1989.
- [22] BERTHET R., PETROSYAN A. and ROMAN B., *Am. J. Phys.*, **70** (2002) 774.
- [23] DALIBARD J., *Lecture Notes at Collège de France, A.Y. 2012-13*
www.phys.ens.fr/~dalibard/2013_CdF.html
- [24] DALIBARD J., GERBIER F., JUZELIŪNAS G. and ÖHBERG P., *Rev. Mod. Phys.*, **83** (2011) 1523.
- [25] CARUSOTTO I. and CIUTI C., *Rev. Mod. Phys.*, **85** (2013) 299.